Estimation and Predictive Control of a Parallel Evaporator Diesel Engine Waste Heat Recovery System

Adamu Yebi, Bin Xu, Xiaobing Liu, John Shutty, Paul Anschel, Zoran Filipi, Simona Onori, and Mark Hoffman

***Abstract*— This paper proposes a real-time capable augmented control scheme for a parallel evaporator organic Rankine cycle (ORC) waste heat recovery system for a heavy-duty diesel engine, which ensures efficient and safe ORC system operation. Assuming a time constant separation between the thermal and pressure dynamics, a nonlinear model predictive control (NMPC) is designed to regulate the mixed working fluid (WF) outlet temperature and the differential temperature between the two parallel evaporator outlets. Meanwhile, the evaporator pressure is regulated by an external PID control. The NMPC is designed using a reduced order, moving boundary control model of the heat exchanger system. In the NMPC formulation, state feedback is constructed from the estimated state via an unscented Kalman filter based on temperature measurements of the exhaust gas and WF at the evaporator outlet. The performance of the proposed control scheme is demonstrated in simulation over an experimentally validated, high fidelity, and physics-based ORC plant model during a transient constant speed and variable load engine drive cycle. The performance of the proposed control scheme (NMPC plus PID) is further validated via comparison with a conventional, multiple-loop PID controlling both the mixed evaporator outlet WF temperature, and the evaporator pressure. The simulation results demonstrate that the proposed control scheme outperforms a multiple-loop PID control in terms of both safety and total recovered thermal energy by up to 12% and 9%, respectively.**

***Index Terms*— Heavy-duty diesel engine, model predictive control, organic Rankine cycle (ORC), unscented Kalman filter (UKF), waste heat recovery (WHR).**

I. Introduction

ABOUT 45% of the energy consumed by a heavy duty diesel engine is wasted via hot exhaust gases and through conduction, convection, and radiation from hot component surfaces [1]. Although it is not technically and economically feasible to recover all waste heat, the increasing need for energy efficiency can be party addressed by adopting waste heat recovery (WHR) technologies. Furthermore, this reused waste heat is "emission free" and would substantially reduce greenhouse gas emissions.

Among existing technologies, organic Rankine cycle (ORC) systems are considered a viable and mature technology for their relative cost effectiveness and high WHR efficiency. The ORC system uses a waste heat source (e.g., engine exhaust) to vaporize working fluid (WF) via a heat exchanger. The vapor phase WF then generates a mechanical power via an expansion device. In most applications, a turbine expander connected with a generator is used to convert the mechanical power to electricity. However, for automotive applications, the expansion device can be used to transfer mechanical power directly to the engine drivetrain. The wide acceptance of ORC technology for WHR can be explained by: 1) its modularity and versatility (i.e., a similar ORC unit can be installed for different applications and heat sources); 2) the technological maturity of the components thanks to the similarities between ORC and refrigeration systems; and 3) its ability to operate efficiently between small and moderate temperature differences. Due to these attributes, an ORC technology has already yielded encouraging results in various settings: automotive WHR [2], combined heat and power plants [3], power generation from renewable heat sources (solar and geothermal) [4], etc.

In automotive WHR alone, ORC technology exhibits superior WHR efficiency (about 15%–25%) [5] relative to competitive technologies, such as thermoelectric generators [6]–[8], turbo compounding [9]–[11], stirling engines [12], [13], and Brayton cycles [14], [15]. As a result, ORC WHR is widely researched for heavy duty vehicles and has yielded various degrees of success, owing to their utilization of long-haul drive cycles [5], [16]–[21]. Cummins achieved 3.6% absolute brake thermal efficiency (BTE) improvement for the on-road tractor-trailer fleet by using both exhaust gas recirculation (EGR) and exhaust gas streams as heat sources in an ORC WHR system [21]. Daimler achieved 2% absolute BTE improvement for on-road tractor-trailer fleet using exhaust gas, engine coolant, and charge air as heat sources [21]. Bosch experimentally obtained 2.1, 5.3, and 9 kW of turbine generated power from B25, B50, and B75 conditions, respectively, while operating a 12L heavy duty engine with an ORC system [20].

Aside from the initial successes of ORC systems in heavy-duty vehicles, implementation challenges prevent the widespread commercial use of ORC-WHR. These challenges

Manuscript received July 9, 2017; accepted August 29, 2017. Manuscript received in final form September 26, 2017. Recommended by Associate Editor Y. Wang. *(Corresponding author: Adamu Yebi.)*

A. Yebi is with the Department of Automotive Engineering, Clemson University-International Center for Automotive Research, Greenville, SC 29607, USA (e-mail: ayebi@clemson.edu).

B. Xu, Z. Filipi, S. Onori, and M. Hoffman are with the Department of Automotive Engineering, Clemson University, Greenville, SC 29607 USA.

X. Liu, J. Shutty, and P. Anschel are with BorgWarner Inc., Auburn Hills, MI 48326 USA.

Color versions of one or more of the figures in this paper are available online at http://ieeexplore.ieee.org.

Digital Object Identifier 10.1109/TCST.2017.2759104

include: 1) developing stable, noncorrosive, and nontoxic WFs for ORC systems; 2) improving expander efficiency; 3) managing the compact component packaging; and 4) obtaining safe and efficient system operation. The first three challenges are related to the system design and publication records indicate that they have garnered significant attention [22]–[27]. However, few works exist which tackle efficient and safe ORC system operation. This challenge requires precise control of ORC system pressure and temperature, and current control strategies often struggle to attain satisfactory performance over transient operating conditions.

The ORC system often undergoes rapid transitions from the nominal operating point to off-design conditions, especially with transient heat sources. Optimal system operation is only possible in a very narrow range of WF evaporating pressure and temperature. The maximum applicable operating temperature is constrained by degradation of the WF while the lower constraint is fixed by condensation of WF in the expansion device/turbine expander. To address the control challenges of maintaining optimal operation within acceptable safety margins, some control design schemes have been proposed in the literature. Many of the existing control schemes focus on the common control approaches: feedback plus feedforward [28], PI-based decentralized control [29], and gain-scheduled PI-type control [30], underlying that the best performance is obtained with regulation of evaporating pressure and superheating temperature. However, such control schemes may not offer optimal or satisfactory results for highly transient heat source profiles for two main reasons: 1) the reference trajectory of evaporation pressure and temperature is generated through steady-state optimization and 2) the disturbance rejection capability of the traditional feedback control methodologies is very limited.

To address the limitations of traditional control strategies, recent works propose the use of advanced control strategies including: nonlinear/linear model predictive control [31], [32], multilinear model predictive control [33], supervisory predictive control [34], and extended prediction self-adaptive control [35]. In most of these works, simulation studies confirmed the superior performance of advanced control strategies over traditional PID control. However, the real-time implementation of advanced control strategies is questionable due to the computational complexity of the intended control algorithm. Most of these studies are focused on precise control which either minimizes the WF superheat or maintains vapor quality close to unity. These ORC control variables are largely assumed to be both safety and performance indicators. Although this assumption is true for ORC systems utilizing a low latent heat WF [36], Xu *et al*. [37] and Xu *et al*. [38] pursued a steady-state power optimization work to determine a theoretical operating point for a selected WF (e.g., ethanol).

To address the aforementioned limitations of the above cited advanced control schemes, two-level control strategies are proposed in the literature. These two-level strategies consider optimal evaporation pressure or temperature trajectory generation in the higher level and reference tracking output feedback control or model predictive control in the lower level [39], [40]. Different methods are considered for reference generation including both offline [41] and online [39], [40] formulations of the optimization problem to maximize the net power within defined safety constraints.

In addition to the well-researched ORC control problem of efficient and safe operation, there are further challenges depending on the ORC system design and configuration. Most common ORC-WHR design architectures for automotive applications include single and double evaporator configurations. In a single evaporator configuration, only the tailpipe (TP) exhaust gas stream is utilized as a heat source with or without an intermediate recuperator [31]. In the double evaporator configuration, two separate evaporators are used to recover heat from both the TP exhaust gas stream and the EGR stream in parallel [32]. For a parallel evaporator ORC system design, a coordinated control effort is needed to split WF mass flowthrough each evaporator. For parallel boiler configurations utilizing a single pump, coordinated actuation of both evaporators for control of the mixed WF temperature at the combined evaporator outlet is not trivial. In addition to the need for coordinated actuation, the coupling of strongly nonlinear system dynamics and the distinctly different time constants of two parallel evaporators interacting with different heat sources makes control of the mixed WF evaporator outlet temperature a difficult problem. In this regard, no work is published except the recent work of [42]. In that prior work, the temperature difference between the individual evaporator outlets is explicitly penalized in a nonlinear model predictive control (NMPC) formulation based on a reduced order, nonlinear, moving boundary (MB) heat exchanger model that aims to regulate the mixed evaporator outlet WF temperature. The control of a parallel evaporator configuration is also considered in [32]. However, separate actuators (bypass valves) are considered for each evaporator, independently returning WF to the reservoir. This ORC system is relatively simple to control compared to the one actuated by a single pump, which is the case considered in the current paper.

In the present contribution, [42] is built upon by extending the proposed NMPC, specifically, as follows.

1) The NMPC formulation is limited to the mixed evaporator outlet WF temperature control and the differential between the individual evaporator outlet temperatures. Meanwhile, a separate PID is designed for evaporator pressure control to reduce the computation burden of the NMPC. This assumes a time constant separation of the pressure and thermal dynamics.
2) A nonlinear state estimation via an unscented Kalman filter (UKF) is pursued for state feedback in the NMPC formulation.
3) A constant speed and variable load (CSVL) engine drive cycle is considered as the transient heat source in simulation.
4) The NMPC is implemented through a real-time possible solver via commercially available software called ACADO [43].
5) New simulation results are included that compare the performance of the augmented NMPC+UKF+PID control algorithm to a conventional PID over a CSVL drive cycle.

MPC is inherently a state feedback control scheme using the current state and a system model for prediction. Thus, for a system model constructed partially from unmeasured states (e.g., WF phaselength and internal wall temperature in the MB model (MBM) of the ORC system), state estimation is must to update the control input based on available output measurements. In the literature, the extended Kalman filter (EKF) is widely used for nonlinear state estimation [44] by successive linearization of the nonlinear model at current predicted states. To compensate for potential estimation accuracy losses due to linearization in the EKF algorithm, the UKF has been proposed to accurately estimate nonlinear system states [45]–[47]. By using the unscented transformation (UT) instead of local linearization, the UKF is reported to offer higher accuracy at computational cost similar to the EKF [48]–[50]. On the other hand, a nonlinear moving horizon estimation (NMHE) based on the history of pervious measurement [51] could potentially compensate for most of the potential EKF/UKF drawbacks such as: nonguaranteed theoretical convergence and estimation failure due to poor initial guesses and tuning parameters. However, the real world practicality of NMHE is questionable because of the associated computational burden. Thus, in this paper, the UKF is utilized for nonlinear state estimation in the NMPC formulation controlling the mixed evaporator outlet WF temperature. The effectiveness of the proposed control scheme (NMPC+UKF+PID) based on the reduced order MBM is then illustrated over an experimentally validated, high fidelity, physics-based ORC plant model.

The remainder of the paper is organized as follows. Section II presents the parallel evaporator ORC system description. Section III presents the heat exchanger thermal and pressure models including both the physics-based, finite volume evaporator model and the reduced order control model or MBM. Section IV discusses the NMPC problem formulation including a summary of the UKF nonlinear state estimation algorithm. Section V provides demonstrative simulation results and discussions. The conclusion is then presented in Section VI.

II. System Description

The ORC is similar to a conventional steam/Rankine cycle except an organic fluid, such as ethanol, replaces water as the WF because of the compatibility between its low temperature vaporization characteristics the low temperature heat source. The ORC system under consideration is schematically shown in Fig. 1. The main components include: high and low pressure pumps, parallel evaporators (boilers) to recover waste heat from TP and EGR line, a turbine expander, and a condenser. The system also contains auxiliary components such as an expansion tank after the condenser, two WF mass flow distribution valves, a turbine inlet valve and a turbine bypass valve.

The ORC system under consideration is coupled with a 13L heavy-duty diesel engine by connecting the evaporators to the TP and EGR circuits. A TP evaporator bypass valve, installed in the ORC system, prevents overheating and subsequent degradation of WF during high load engine operation. The ORC EGR evaporator replaces the stock EGR intercooler from the engine assembly. Ethanol serves as the WF because

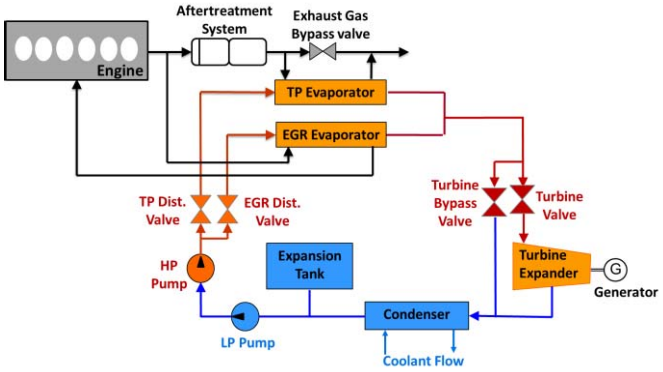

Fig. 1. Schematic of ORC system with paralel boiler for WHR.

of its favorable thermal characteristics and environmental friendliness.

The pump circulates WF through the evaporator where it undergoes phase changes from pure liquid to two phase (liquid plus vapor) and finally to vapor at high pressure by absorbing thermal energy from the heat source. The high pressure WF vapor then expands through the turbine, facilitating work extraction through either electrical generation or direct utilization of the mechanical power. Finally, the WF vapor flows from the turbine expander through the condenser where it transitions back to liquid phase. This is one complete ORC flow cycle. A turbine inlet valve and a turbine bypass valve work together to ensure safe turbine expander operation away from the two-phase WF saturation regime and smooth system transients.

III. ORC System Modeling

To facilitate the control design, physics-based models are developed for the key ORC system components. Both the high-fidelity physics-based and reduced control-oriented models are detailed in this section. Emphasis is placed on the key ORC components such as the evaporators and compressible pipe volumes.

A. Evaporator

The evaporators are the key ORC system components, facilitating energy transport from the heat source to the WF. Heat transfer inside each evaporator is modeled via conservation of mass and energy balance. The heat exchanger model assumes a helical coil evaporator construction where the hot gas and WF are separated by a wall. As a result, the energy balance is considered in three separate media: the WF, the exhaust gas, and wall separating them. In addition, WF mass conservation is considered to simulate the mass flow rate as the ethanol experiences phase change phenomena. To simplify the heat exchanger model, the following three assumptions are made: 1) heat conduction in the axial direction of the evaporator is neglected for all media (WF, wall, and hot gas); 2) vapor inside the heat exchanger is assumed to be incompressible; and 3) the wall temperature is assumed to be uniform in the radial direction. For an extended discussion

and other modeling considerations, one can refer to [19]. The following coupled, 1-D partial differential equations (PDEs) in (1)–(4) summarize the evaporator model [19], [29], [52].

Conservation of mass (WF)

$$A_f \frac{\partial \rho_f}{\partial t} + \frac{\partial \dot{m}_f}{\partial z} = 0 \tag{1}$$

where ρ_f and $\dot{m}_f$ denote WF density and mass flow rate, respectively, A_f is the contact area between the wall and the WF, and z is a spatial axis in the WF flow direction.

Conservation of energy (WF)

$$\rho_f V_f \frac{\partial h_f}{\partial t} = -\dot{m}_f L \frac{\partial h_f}{\partial z} + A_f U_f (T_w - T_f) \tag{2}$$

where V_f and h_f denote the WF volume and enthalpy, respectively, L is the total evaporator length, U_f is the heat transfer coefficient between wall and WF, T_w is the wall temperature, and T_f is the WF temperature.

Conservation of energy (gas side)

$$\rho_g C_{pg} V_g \frac{\partial T_g}{\partial t} = \dot{m}_g C_{pg} L \frac{\partial T_g}{\partial z} + A_g U_g (T_w - T_g) \tag{3}$$

where ρ_g, C_{pg}, V_g, T_g, and $\dot{m}_g$ denote the exhaust gas density, heat capacity, volume, temperature, and mass flow rate, respectively. Additionally, A_g is the contact area between wall and exhaust gas, and U_g denotes the heat transfer coefficient between wall and exhaust gas. For the exhaust gas energy balance in (3), a change is made from [19]. For numerical tractability, the exhaust gas enthalpy is approximated by $h_g = C_{pg} T_g$. The density and specific heat capacity of the exhaust gas are considered constant while WF density changes as a function of enthalpy.

Conservation of energy (wall)

$$\rho_w C_{pw} V_w \frac{\partial T_w}{\partial t} = -A_f U_f (T_w - T_f) - A_g U_g (T_w - T_g) \tag{4}$$

where ρ_w, C_{pw}, and V_w denote the wall temperature, heat capacity, and volume, respectively.

B. Pipes Containing Compressible Vapor

Evaporator pressure dynamics are derived from modeling the compressible WF vapor in the pipes between the evaporators and the turbine. Compressibility is necessary to accurately describe the WF pressure, temperature, and mass inside the pipe volume. Conservation principles (mass/energy) are applied to this compressible vapor volume, as summarized in the following:

$$\frac{dm_f}{dt} = \dot{m}_{f,\text{in}} - \dot{m}_{f,\text{out}} \tag{5}$$

$$u_f \frac{dm_f}{dt} + m_f c_v \frac{dT}{dt} = \dot{H}_{\text{in}} - \dot{H}_{\text{out}} \tag{6}$$

where m_f, u, c_v, and T are the WF mass, specific internal energy, specific heat capacity, and temperature, respectively. Meanwhile, $\dot{m}_{\text{in}}$, $\dot{m}_{\text{out}}$, $\dot{H}_{\text{in}}$, and $\dot{H}_{\text{out}}$ are the inlet and outlet WF mass flow rates and enthalpy flow rates, respectively. In order to calculate the pressure, the ideal gas law is utilized with the assumption that the vapor WF is an ideal gas [53]

$$\frac{RT}{V}\frac{dm_f}{dt} + \frac{p}{T}\frac{dT}{dt} - \frac{dp}{dt} = 0 \tag{7}$$

where R is the ideal gas constant, V is the vapor volume, and p is the evaporator pressure. Thus, (5)–(7) summarize the pressure dynamics.

C. Pump and Turbine

The pump and turbine dynamics are fast relative to the evaporator dynamics. As a result, they are modeled by algebraic equations and maps. For detailed descriptions of the pump and turbine models, the remaining component models, and the experimental model validation, one can consult [19]. This paper focuses on the power generated and consumed by the turbine and pump, respectively. The power consumption by a positive displacement pump is described as follows:

$$P_{\text{Pump}} = \frac{\dot{m}_{\text{pump}} (p_{\text{out,pump}} - p_{\text{in,pump}})}{\rho \eta_{\text{is,pump}}} \tag{8}$$

where $\dot{m}_{\text{pump}}$ is the WF mass flow rate through pump; $\rho$is the pump upstream density; $p_{\text{in,pump}}$ and $p_{\text{out,pump}}$ are upstream and downstream pressure; and $\eta_{\text{is,pump}}$ is the isentropic efficiency. Note that a pump mass flow rate map from the manufacturer is utilized in the simulation study.

Power generated from the mechanically coupled turbine expander is described as follows:

$$P_{\text{Turb}} = \eta_{\text{conv}} \eta_{\text{em}} \eta_{\text{thermal}} \dot{m}_{\text{in}} (h_{\text{in}} - h_{\text{out}}). \tag{9}$$

The thermal efficiency, η_{thermal}, is determined from a manufacturer-proprietary map based on three inputs: inlet pressure, turbine speed, and the pressure ratio across the turbine. Outlet enthalpy, h_{out}, is also interpolated from a 2-D map using turbine outlet pressure and entropy as inputs. η_{eg} is the electric generator efficiency, and η_{conv} is the conversion efficiency.

D. Control-Oriented Evaporator Model

The finite volume discretization technique is often used in simulation to convert the coupled PDEs in (1)–(4) into a set of ordinary differential equations (ODEs). The direct spatial PDE discretization returns large ODE systems that are not readily applicable for real-time control and estimation purposes. For control design purposes, a three-cell discretization system using an MB approach is considered. The MBM dynamically tracks the lengths of the different WF phases (liquid, two phase, and vapor) along the evaporator length while applying the same governing differential equations (1)–(4) to each region using control volumes [54]. A schematic of the MBM discretization is shown in Fig. 2.

Assuming homogenous thermodynamic properties along each control volume (phase region), lumped differential equations are derived by integrating the mass and energy conservation equations. Following the derivation procedure detailed in [54], a sixth-order ODE system is derived. The exhaust gas dynamics are neglected due to their fast transient characteristics. The system of differential equations is summarized in the following.

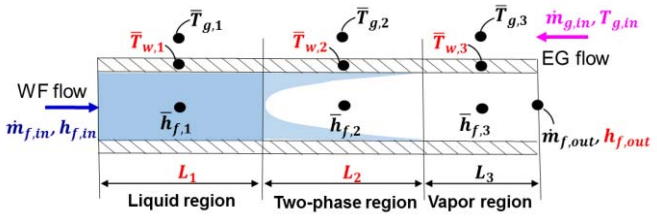

Fig. 2. MB discretization schematic of the evaporator.

1) Liquid Region: Phaselength dynamics in liquid phase (L_1)

$$\bar{\rho}_{f,1}(\bar{h}_{f,1}-h_{f,1})\frac{dL_1}{dt} = -\frac{1}{2}AL_1\left[\bar{\rho}_{f,1}+\frac{\partial\bar{\rho}_{f,1}}{\partial h}(\bar{h}_{f,1}-h_{f,1})\right]\frac{dh_{\text{in}}}{dt} + \dot{m}_{f,\text{in}}(h_{f,\text{in}}-h_{f,1})+\pi d_{\text{tube}}L_1U_{\text{fw},1}(\bar{T}_{w,1}-\bar{T}_{f,1}) \tag{10a}$$

Wall temperature dynamics ($\bar{T}_{w,1}$)

$$Ac_p\rho_wL_1\frac{d\bar{T}_{w,1}}{dt}+Ac_p\rho_w(\bar{T}_{w,1}-\bar{T}_{w,l})\frac{dL_1}{dt} = \pi d_{\text{tube}}L_1U_{fw,1}(\bar{T}_{f,1}-\bar{T}_{w,1}) + \eta\pi d_{\text{shelleqv}}L_1m_{\text{HTC}}U_{g,w}(\bar{T}_{\text{TP},1}-\bar{T}_{w,1}) \tag{10b}$$

2) Two-Phase Region: Phaselength dynamics in liquid phase (L_2)

$$A[\bar{\rho}_{f,1}(h_{fl}-h_{fg})]\frac{dL_1}{dt}+A(1-\bar{\gamma})[\rho_{f,l}(h_{f,l}-h_{fg})]\frac{dL_2}{dt} = -\frac{1}{2}AL_1\frac{\partial\bar{\rho}_{f,1}}{\partial h}\frac{dh_{\text{in}}}{dt}(h_{fl}-h_{fg})+\dot{m}_{f,\text{in}}(h_{f,l}-h_{f,g}) + \pi d_{\text{tube}}L_2U_{fw,2}(\bar{T}_{w,2}-\bar{T}_{f,2}) \tag{11a}$$

Wall temperature dynamics ($\bar{T}_{w,2}$)

$$Ac_p\rho_wL_2\frac{d\bar{T}_{w,2}}{dt}+Ac_p\rho_w(\bar{T}_{w,l}-\bar{T}_{w,g})\frac{dL_1}{dt} + Ac_p\rho_w(\bar{T}_{w,2}-\bar{T}_{w,g})\frac{dL_2}{dt} = \pi d_{\text{tube}}L_2U_{fw,1}(T_{\text{sat}}-\bar{T}_{w,2}) + \eta\pi d_{\text{shelleqv}}L_2m_{\text{HTC}}U_{g,w}(\bar{T}_{\text{TP},2}-\bar{T}_{w,2}) \tag{11b}$$

3) Vapor Region: Evaporator outlet enthalpy dynamics ($h_{f,\text{out}}$)

$$\begin{aligned}&A[\bar{\rho}_{f,3}(h_{f,\text{out}}-\bar{h}_{f,3})+\bar{\rho}_{f,1}(h_{f,g}-h_{f,\text{out}})]\frac{dL_1}{dt}\\&+A[\bar{\rho}_{f,3}(h_{f,\text{out}}-\bar{h}_{f,3})+((1-\bar{\gamma})\rho_{f,l}+\bar{\gamma}\rho_{f,g})\\&\times(h_{f,g}-h_{f,\text{out}})]\frac{dL_2}{dt}+\frac{1}{2}AL_3\\&\times\left[\bar{\rho}_{f,3}-\frac{\partial\bar{\rho}_{f,3}}{\partial h}(h_{f,\text{out}},\bar{h}_{f,3})\right]\frac{dh_{f,\text{out}}}{dt}\\&=-\frac{1}{2}AL_1\left[\frac{\partial\bar{\rho}_{f,1}}{\partial h}(h_{fg}-h_{f,\text{out}})\right]\frac{dh_{\text{in}}}{dt}+\dot{m}_{f,\text{in}}(h_{f,g}-h_{f,\text{out}})\\&+\pi d_{\text{tube}}L_3U_{fw,3}(\bar{T}_{w,3}-\bar{T}_{f,3})\end{aligned} \tag{12a}$$

Wall temperature dynamics ($\bar{T}_{w,3}$)

$$\begin{aligned}&Ac_p\rho_wL_3\frac{\partial\bar{T}_{w,3}}{\partial t}+Ac_p\rho_w(\bar{T}_{w,g}-\bar{T}_{w,3})\frac{dL_1}{dt}\\&+Ac_p\rho_w(\bar{T}_{w,g}-\bar{T}_{w,3})\frac{dL_2}{dt}\\&=\pi d_{\text{tube}}L_3U_{fw,3}(\bar{T}_{f,3}-\bar{T}_{w,3})\\&+\eta\pi d_{\text{shelleqv}}L_3m_{\text{HTC}}U_{g,w}(\bar{T}_{\text{TP},3}-\bar{T}_{w,3})\end{aligned} \tag{12b}$$

where $L_3 = L-(L_1+L_2)$; d_{tube} and d_{shelleqv} are the heat exchanger hydraulic diameters on the WF and exhaust gas sides, respectively; m_{HTC} is a multiplier to enhance the gas side heat transfer coefficient, and η is a multiplier that account for heat loss between the exhaust gas side and the ambient. The subscripts $i = 1, 2, 3$ stand for liquid, two-phase and vapor regions, respectively.

The exhaust gas temperature evolution is predicted by the following algebraic equations:

$$\bar{T}_{g,1} = \frac{[\pi d_{\text{tube}}L_1U_{g,w}\bar{T}_{w,1}+\dot{m}_gC_{pg}\{2\bar{T}_{g,2}-2\bar{T}_{g,3}+T_{g,\text{in}}\}]}{\dot{m}_gC_{pg}+\pi d_{\text{tube}}L_1U_{g,w}} \tag{13a}$$

$$\bar{T}_{g,2} = \frac{[\pi d_{\text{tube}}L_2U_{g,w}\bar{T}_{w,2}+\dot{m}_gC_{pg}\{2\bar{T}_{g,3}-T_{g,\text{in}}\}]}{\dot{m}_gC_{pg}+\pi d_{\text{tube}}L_2U_{g,w}} \tag{13b}$$

$$\bar{T}_{g,3} = \frac{[\pi d_{\text{tube}}L_3U_{g,w}\bar{T}_{w,3}+\dot{m}_gC_{pg}T_{g,\text{in}}]}{\dot{m}_gC_{pg}+\pi d_{\text{tube}}L_3U_{g,w}} \tag{13c}$$

Remark I: The MBM summarized in (10)–(13) assumes the coexistence of all three phases of WF along the evaporator.

Remark II: The heat exchanger model described above can be adapted for both evaporators (TP and EGR).

For control formulation purposes, the resulting differential and algebraic equations in (10)–(13) can be written in the standard nonlinear state space form

$$\begin{cases}\dot{x} = f(x,z,w,u)\\0 = g(x,z,w)\end{cases} \tag{14}$$

where $x = [L_1, \bar{T}_{w,1}, L_2, \bar{T}_{w,2}, \bar{T}_{w,3}, h_{f,\text{out}}]^T$ is a dynamic state vector; $z = [\bar{T}_{g,1}, \bar{T}_{g,2}, \bar{T}_{g,3}]^T$ is an algebraic state vector; $u = \dot{m}_{f,\text{in}}$ is a control input; and $w = [\dot{m}_g, T_{g,\text{in}}]^T$ is an exogenous disturbance vector (input from the engine to the ORC system).

IV. Closed-Loop Control Design

In this section, the proposed closed-loop control algorithm is formulated for safe and efficient ORC-WHR system operation during transient operation. Specifically, the control scheme includes: 1) a NMPC to regulate the mixed evaporator outlet WF temperature; 2) an external PID loop for evaporator outlet pressure control; and 3) a nonlinear state estimation via an UKF. The proposed NMPC addresses three fundamental ORC system control challenges. The first is the highly nonlinear evaporator dynamics that often hinder control via classical approaches. The second is the set of system states, and input–output constraints that must be satisfied for safety considerations. The last challenge is the need to satisfy multiple control objectives, namely, maximizing the net waste heat power recovery while maintaining safe operation.

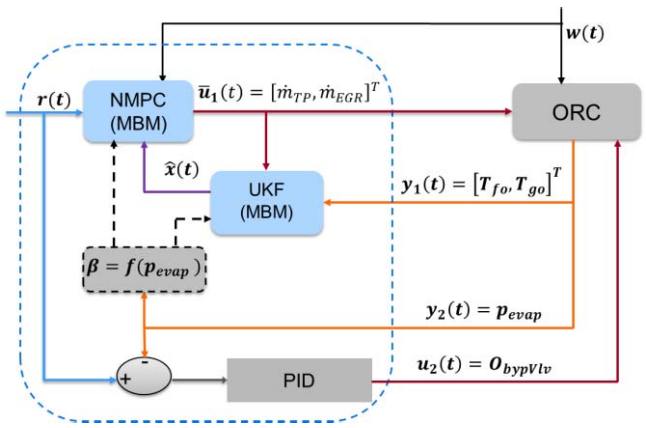

Fig. 3. Closed-loop control scheme for ORC-WHR (β is model paramter vectors updated based on system pressure; T_{fo}&T_{go} are evaporator outlet WF and exhaust gas temperature, respectively; and O_{bypVlv} is bypass valve opening).

For similar control challenges, the model predictive control approach has gained traction as a successful control strategy because it handles multivariable problems naturally and can reject any measurable disturbance ahead of time [55].

For the ORC system under consideration, the primary temperature regulation control input is the pump speed, which adjusts the WF mass flow. To split the mass flowthrough the parallel evaporators, two distribution valves are utilized for intermediate actuation. The turbine bypass valve is considered as an actuation to regulate the evaporator outlet pressure. A schematic of the proposed closed-loop control scheme that describes the input–output configuration is shown in Fig. 3.

A. NMPC Formulation

In the following NMPC formulation, both WF mass flows, $\dot{m}_{\text{TP}}$ and $\dot{m}_{\text{EGR}}$, are control inputs and a nonlinear map between the distribution valve opening and mass flow is assumed. Similarly, pump speed is correlated with total WF mass flow, and conservation of WF mass flow is applied downstream, namely, $\dot{m}_{\text{pump}} = \dot{m}_{f,\text{TP}} + \dot{m}_{f,\text{EGR}}$. The NMPC problem is formulated as a finite horizon optimal control problem subjected to nonlinear system dynamics and both input and state constraints. The NMPC formulation for ORC system is given

$$\begin{aligned}
&\min_{\bar{u}(.),\bar{x}(.)} \quad J(\hat{x}(t_i), \bar{u}(.)) \\
&\text{s.t:} \begin{cases} \dot{\bar{x}}(\tau) = f(\bar{x}(\tau), \bar{z}(\tau), u(\tau), w(t_i)), \quad \bar{x}(t_i) = \hat{x}(t_i) \\ 0 = g(\bar{x}(\tau), \bar{u}(\tau), w(t_i)), \\ \bar{y}(\tau) = h(\bar{x}(\tau), \bar{z}(\tau), \bar{u}(\tau), w(t_i)) \end{cases} \\
&\quad y^{lb} \le \bar{y}(\tau) \le y^{ub} \quad \forall \tau \in [t_i, t_i + T_p] \\
&\quad u^{lb} \le \bar{u}(\tau) \le u^{ub} \quad \forall \tau \in [t_i, t_i + T_c] \\
&\quad \bar{u}(\tau) = \bar{u}(t_i + T_c) \quad \forall \tau \in [t_i + T_c, t_i + T_p] \\
&\quad x^{lb} \le \bar{x}(\tau) \le x^{ub}
\end{aligned} \tag{15}$$

where $J : \mathbb{R}^n \times \mathbb{R}^m \to \mathbb{R}$ is the cost function for optimization; n and m are dimension of state and input; T_p and T_c denote the prediction and control horizon, respectively, with $T_c \le T_p$; the superscripts lb and ub indicate the lower and upper bounds of the constrained variables, respectively; the bar $(\bar{\cdot})$ denotes predicted variables based on the control model using the estimated state feedback, $\hat{x}(t_i)$, and predicted input $\bar{u}$.

The main goal of the optimization problem for the ORC-WHR system is to maximize the energy recovered from the waste heat. To achieve this goal, the objective function can be defined directly as the net ORC system power, or indirectly in terms of control trajectory tracking to maximize the energy recovery. Although a few efforts [31] consider the direct option for objective function formulation, a larger volume of existing works on ORC applications [32], [39] utilize cost functions that track a predefined trajectory for numerical reasons. This is because a nonquadratic objective function (e.g., net power) may return nonunique and sometimes infeasible solutions, possibly leading to unnecessary/excessive system actuation. For WHR-ORC systems that utilize a low latent WF (e.g., ethanol), a reference trajectory for power maximization could be a mixed evaporator outlet temperature close to saturation temperature. The temperature trajectory approach is considered in this paper for its numerical tractability. To address the control challenge of coordinated mass flow distribution through the parallel evaporators evaporator, the NMPC cost function penalizes the difference between evaporator WF exit temperatures in addition to the direct mixed evaporator temperature control for power maximization [40]. This is described as a convex cost function of the form

$$J = \int_{t_i}^{t_i+T_p} \left\{ (I-B) \frac{(T_d - T_{f,\text{mix}})^2}{T_{\text{max}}^2} + B \frac{(T_{f,\text{TP}} - T_{f,\text{EGR}})^2}{T_{\text{max}}^2} \right\} d\tau \tag{16}$$

where $T_{f,\text{mix}}$ is mixed evaporator outlet temperature; T_d is desired temperature reference for control; $B \in \mathbb{R}$ is a positive definite weighting matrix; and T_{max} is maximum temperature. The mixed temperature is calculated using thermodynamic tables at a given evaporator pressure and the mixed enthalpy from both parallel evaporators $(p, h_{f,\text{mix}})$. The mixed enthalpy is calculated from the energy balance equation given in

$$\dot{m}_{\text{pump}} h_{f,\text{mix}} = \dot{m}_{f,\text{TP}} h_{f,\text{TP}} + \dot{m}_{f,\text{EGR}} h_{f,\text{EGR}}. \tag{17}$$

The constraints in (15) include physical actuation limitations and safe ORC system operation. The actuator limitations are defined by upper and lower bounds on input values (u^{lb}, u^{ub}) as well as on the rates of input change $(\delta\dot{u}^{lb}, \delta\dot{u}^{ub})$. For safe operation, the maximum WF temperature is limited to avoid ethanol dissociation and degradation. The minimum vapor quality at the turbine inlet is set to be greater than one to avoid ethanol condensation in the turbine expander. These safety conditions are treated as output constraints (y^{lb}, y^{ub}).

In order to meet real-time implementation constraints with NMPC, the ACADO open source software package [43] is used for efficient real-time code generation. The ACADO tool has been used for dynamic optimization and estimation problems including constrained NMPC [56]. ACADO exports an efficient C++ code based on a direct multiple shooting algorithm. The resulting real-time implementable code exploits the structure of the specific optimization problem by avoiding

irrelevant computations. The effectiveness of the ACADO code generation tool for this ORC WHR application is shown in the simulation result section in terms of NMPC computation time.

B. Unscented Kalman Filter

The NMPC formulation in (15) assumes the availability of full state information for feedback through either direct measurement or estimation. Full state estimation via an UKF algorithm is considered in this paper due to practical limitations of measuring some control model states, namely, the lengths of each WF phase and the internal evaporator wall temperature. In this section, the practical UKF implementation on a discrete nonlinear system is briefly reviewed and summarized. For a more detailed discussion, refer to [46].

Consider the following nonlinear discrete system, with additive stochastic noise:

$$x_k = F(x_{k-1}) + q_{k-1} \tag{18a}$$

$$z_k = H(x_k) + v_k \tag{18b}$$

where $x_k \in \Re^n$ is n-dimensional state variable and $z_k \in \Re^m$ is m-dimensional system output. $F \in \Re^n$ is the discretized nonlinear system function and $H \in \Re^m$ is the nonlinear output function vector. q_k and v_k represent the process noise and output noise, with covariance matrices Q_k and R_k, respectively, where k is the time index.

The UKF shares the same prediction-correction structure as that of an EKF. Instead of the successive linearization used in the EKF, the UT is used in UKF. The UT is a method for calculating the mean and covariance of a random variable, which undergoes a nonlinear transformation. For a random variable vector x, with mean x_m and covariance P_x, the UT through a nonlinear function, $y = g(x)$, is used to predict the mean and covariance of the transformed random variable y. This is facilitated by defining a set of sigma points that capture the mean and covariance of the initial vector random variable x.

Assuming a known initial state estimation $\hat{x}$, ($\hat{x} = x_m$) and the corresponding covariance, P_x, at $k = 1$, the UKF implementation is detailed in three steps in the following [46], [57].

Step 1: Generate a set of sigma points, χ^i_{k-1}, and the associated weights, W_i, for $i = 0, \ldots, 2n$

$$\begin{cases} \chi^0_{k-1} = \hat{x}_{k-1} \\ \chi^i_{k-1} = \hat{x}_{k-1} + \left(\sqrt{(n+\lambda)P^+_{xk-1}}\right)_i & \forall i = 1, \ldots, n \\ \chi^i_{k-1} = \hat{x}_{k-1} - \left(\sqrt{(n+\lambda)P^+_{xk-1}}\right)_i & \forall i = n+1, \ldots, 2n \end{cases} \tag{19}$$

$$\begin{cases} W^{(m)}_0 = \lambda/(n+\lambda) \\ W^{(c)}_0 = \lambda/(n+\lambda) + (1-\alpha^2+\beta) \\ W^{(m)}_i = W^{(c)}_i = 1/(n+\lambda) \quad \forall i = 1, \ldots, 2n \end{cases} \tag{20}$$

where $\lambda = \alpha^2(n+\kappa) - n$ is a scaling parameter, α determines the spread of the sigma points around mean value—usually small values are utilized (e.g., $0 < \alpha \leq 1$); $\kappa = 3 - n$ is a secondary scaling parameter; $\beta = 2$ is used assuming a Gaussian distribution of the random variable; and finally, $W^{(m)}$ and $W^{(c)}$ are the weights for mean and covariance prediction from the sigma points.

Step 2: Propagate the generated sigma points in step 1 through the system state equation and observation model in (18) and predict the mean and covariance of the transformed/forecast sigma points through both the state equation and the observation model. In the following the superscript f is used to distinguish forecast sigma points.

1) Propagate the sigma points through the state equation

$$\chi^f_{k,i} = F\left(\chi^i_{k-1}\right). \tag{21a}$$

2) Mean and covariance of the transformed sigma points

$$\hat{x}^-_k = \sum_{i=0}^{2n} W^{(m)}_i \chi^f_{k,i} \tag{21b}$$

$$P^-_{xk} = \sum_{j=0}^{2n} W^{(c)}_i \left(\chi^f_{k,i} - \hat{x}_k\right)\left(\chi^f_{k,i} - \hat{x}_k\right)^T + Q_{k-1}. \tag{21c}$$

3) Propagate the sigma points through the observation model

$$z^f_{k,i} = H\left(\chi^i_k\right). \tag{22a}$$

4) Mean and covariance of the transformed observation

$$\hat{z}_k = \sum_{i=0}^{2n} W^{(m)}_i z^f_{k,i} \tag{22b}$$

$$P_{zk} = \sum_{j=0}^{2n} W^{(c)}_i \left(z^f_{k,i} - \hat{z}_k\right)\left(z^f_{k,i} - \hat{z}_k\right)^T + R_k. \tag{22c}$$

Step 3: Correct the predicted mean and covariance by calculating the cross-covariance between $\tilde{x}_k$ and $\tilde{z}_k$ and correction gain K_k.

1) Cross-covariance

$$P_{xzk} = \sum_{j=0}^{2n} W^{(c)}_i \left(\chi^f_{k,i} - \hat{x}_k\right)\left(z^f_{k,i} - \hat{z}_k\right)^T. \tag{23a}$$

2) Gain K_k

$$K_k = P^+_{xk} P^{-1}_{zk}. \tag{23b}$$

3) Updated the mean state and covariance

$$\hat{x}^+_k = \hat{x}^-_k + K_k(z_k - \hat{z}_k) \tag{23c}$$

$$P^+_{xk} = P^-_{xk} - K_k P_{zk} K^T_k. \tag{23d}$$

The UKF algorithm summarized in (19)–(23) completes a discrete time step UKF state estimation.

V. Results and Discussion

In this section, simulation results are presented to demonstrate the proposed closed-loop control performance. The simulated plant model is the coupled PDE system of equations given in (1)–(4) including the pressure model summarized in (5)–(7). For a stable numerical simulation of the high fidelity plant model, each PDE in (1)–(4) is discretized into 50 finite volume cells, resulting in a total

of 300 ODE dynamics and an additional 100 differential algebraic equations (DAE). The 100 DAEs are derived from the gas side PDE in (3) neglecting the gas dynamics due to their fast transient characteristics. The experimental validation of this high fidelity heat exchanger model is discussed in [19]. The reduced order MBM summarized in (11)–(14) is then utilized for the NMPC optimization and UKF state estimation.

The UKF algorithm summarized in (18)–(23) is implemented in Simulink to estimate the unmeasurable states of the MB control model using measured evaporator outlet WF and exhaust gas temperatures in the presence of process and measurement noise. A white, zero mean, and Gaussian noise of covariance $R_k = 0.5$ is added to the simulated plant model to mimic actual temperature measurement data. The mismatch between the reduced order control model and the high fidelity, physics-based plant model inherently produces process noise. The process noise covariance matrix $[Q_k = \text{diag}(1e^{-5} * [0.24, 0.24, 25.6e5, 8.5, 8.5, 3.4])$ is used in the UKF estimation to effectively cancel out the process and measurement noise. The estimated states via the UKF are used to update the control input when solving the optimal control problem in (15) using a real-time implementable solver via ACADO. In ACADO, the NMPC prediction horizon step is set to 50, totaling 20 s of future prediction time. With this prediction time length, the slow thermal dynamics of the ORC system can be captured for a given engine operating condition. The NMPC weight matrix is tuned offline to find the best tracking performance.

The UKF prediction step is solved with an implicit numerical integrator that is suitable for solving DAEs with stiff characteristics. The ORC system has stiff dynamics due to the very small mass of WF in the vapor phase regions. The integration method is discussed in [42], and a similar method is also discussed in [58].

The diesel engine and ORC WHR system are subjected to a simulated CSVL transient cycle to demonstrate the performance of the proposed closed-loop control scheme over a transient engine operating conditions. The engine speed, torque, and EGR rate profiles for the CSVL are shown in Fig. 4. This cycle is specifically constructed to approximate long-haul tractor-trailer operation, which is a prime candidate for ORC WHR due to sustained periods of moderate torque demand. As such, the engine speed is focused into a relatively narrow range while engine torque is highly transient. This simulates maintaining a near constant highway speed without needing to shift the transmission. For low to moderate road grade changes, the driver simply varies the engine torque to maintain constant speed. The EGR and TP exhaust gas mass flow rates and temperatures shown in Fig. 5 are obtained from a GT-POWER engine model simulation for the given CSVL engine profile. The GT-POWER model is calibrated and validated against the experimental engine accompanying the real-world ORC system [59]. This includes the addition of thermal inertia to appropriately dampen the exhaust gas and EGR temperature trajectories relative to mass flow changes.

The simulation results presented in this section consider the following two assumptions: 1) the ORC system is initialized in warm conditions, namely, all three phases of WF are present

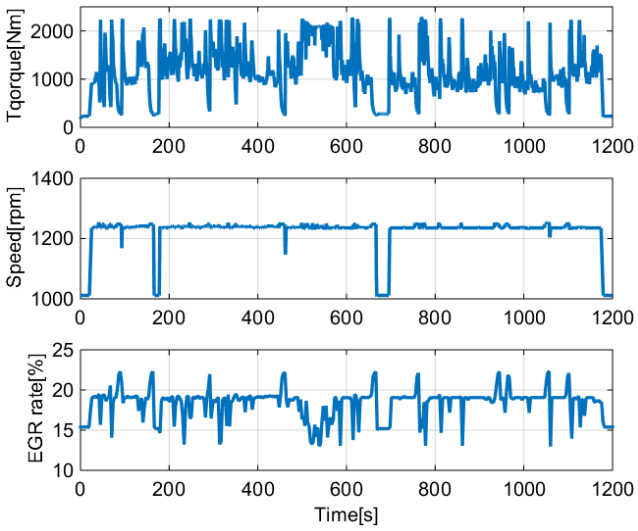

Fig. 4. CSVL transient profiles for engine operating condition.

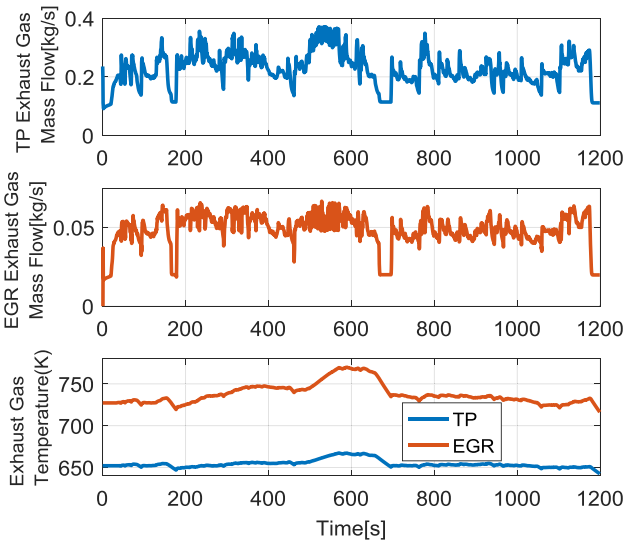

Fig. 5. Engine exhaust gas conditions for the CSVL drive cycle.

in the MBM and 2) a constant condenser outlet temperature of 30 °C is considered in the entire simulation. This assumption is implemented because the experimental ORC WHR apparatus utilized to calibrate the models is configured with open loop condenser cooling via the facility water supply. Although the condenser shares the same modeling assumptions as the evaporator, it is not exposed to the exogenous disturbances of transient engine exhaust mass flow and exhaust gas temperature. As a result, it is assumed that the condenser can be effectively controlled by an external PID control.

The simulation results are presented in two parts. First, the performance of the proposed augmented control (NMPC + UKF + PID) is demonstrated in Figs. 6–9. The mixed evaporator outlet WF temperature set point is controlled through the NMPC+UKF and the evaporator outlet pressure set point is controlled externally via PID. The real-time PID control gains are interpolated from a scheduled control gain map based on measured evaporator pressure and mixed evaporator WF temperatures.

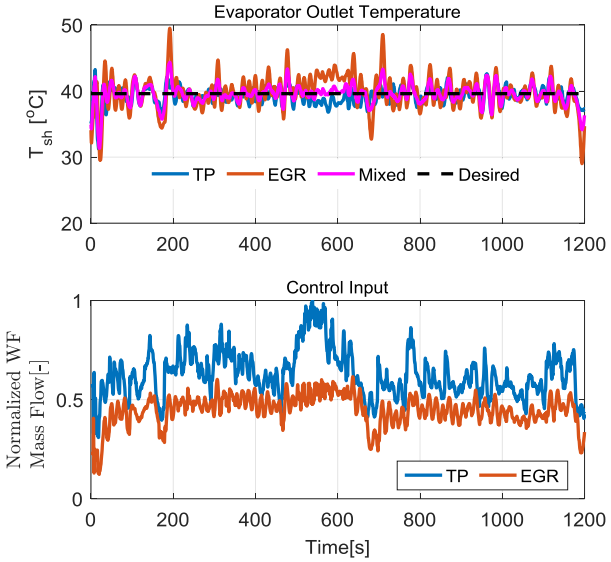

Fig. 6. Evaporator outlet WF temperature control response and corresponding control input of normalized WF mass flow.

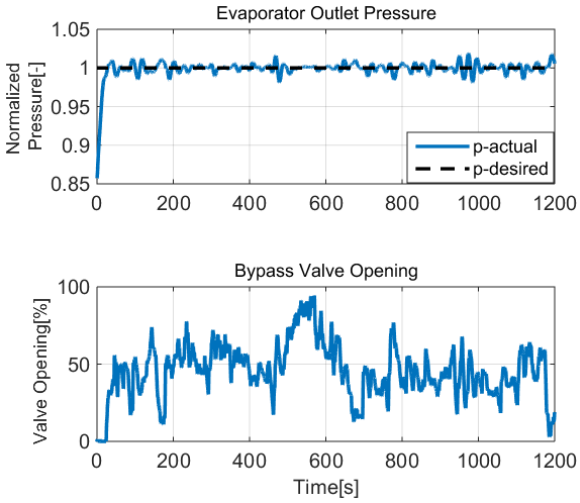

Fig. 7. Evaporator outlet pressure control response and corresponding control input of bypass valve opening percentage.

In the second part of the simulation results, Figs. 10 and 11, the performance of the proposed control scheme is compared against a conventional multiple-loop PID controller design, which incorporates independent PID controls for the mixed evaporator outlet WF temperature and the evaporator outlet pressure. This conventional PID control design utilizes the same control strategy as the NMPC, operating on the evaporator outlet WF temperature. Namely, two separate PID controllers are implemented. The first PID directly controls the mixed WF temperature set point and the second PID controls the temperature difference between the two evaporator outlets. In addition, a feedforward controls are added for both PID loops. The control gains for both PIDs are interpolated from a scheduled control gain map based on measured evaporator pressure and calculated exhaust power.

A. Performance Studies With the Proposed Control (NMPC+UKF+PID)

Fig. 6 shows the NMPC mixed evaporator outlet WF temperature control performance along with the control input of WF mass flow. The mixed WF temperature is precisely controlled around the constant set point value of 40 °C superheat temperature (T_{sh}) by the proposed control scheme with a tolerable temperature deviation of ±10 °C. Note that the superheat temperature (T_{sh}) reference in the following simulation results is calculated by subtracting the time varying saturation temperature from the actual temperature value.

The maximum 10 °C deviation is observed only at those points where an aggressive exhaust gas mass flow input change is introduced, which exemplifies the NMPC disturbance rejection capability. The NMPC disturbance rejection capability is well explained by the control input transient response, which mimics the transient frequency of the exogenous disturbance input (engine exhaust gas mass flow) shown in Fig. 5. In this simulation, the input disturbance is assumed to be constant over the NMPC prediction horizon and updated at every feedback sample time of 0.2 s. If the engine operating condition (disturbance input) is known in the future prediction from some kind of disturbance estimation, the control performance could be improved through the implementation of a future disturbance input trajectory rather than holding the input constant. The EGR evaporator experienced increased temperature deviations relative to the TP evaporator, as shown in Fig. 6. This is due to thermal inertia disparity between EGR and TP evaporators. Namely, the EGR evaporator is smaller in size than the TP evaporator.

Fig. 7 examines the PID control performance for a constant evaporator outlet pressure set point while controlling the mixed evaporator outlet WF temperature via NMPC to a constant superheat level above the time-varying WF saturation temperature. A precise pressure control is achieved by the external PID loop with a short control response time of about 12 s. The corresponding PID control input is bypass valve opening percentage, also shown in Fig. 7. Note that for the precise evaporation pressure control at a desired set point, turbine valve opening may require an upper bound. Otherwise, the system may not build enough pressure for proper turbine operation. In this simulation, the turbine valve is limited to 40% while adjusting the bypass valve opening based on the PID pressure control.

For pressure control, the bypass valve opening is adjusted directly based on the PID gains while mass flowthrough TP and EGR evaporators are computed from the NMPC formulation. For computational efficiency, a map converts the desired mass flows into the two distribution valve openings (TP and EGR).

The performance of the proposed nonlinear state estimation is shown in Fig. 8 using the simulated evaporator outlet WF temperature results from the full fidelity ORC model. The estimated temperature converges to the measured temperature within 4 s for an initial condition deviation of over 20 °C, and effectively filters the added noise. Similar performance is observed for the evaporator outlet exhaust gas temperatures. Here, the estimation performance evaluation is limited to the evaporator outlet temperature because of the state variable

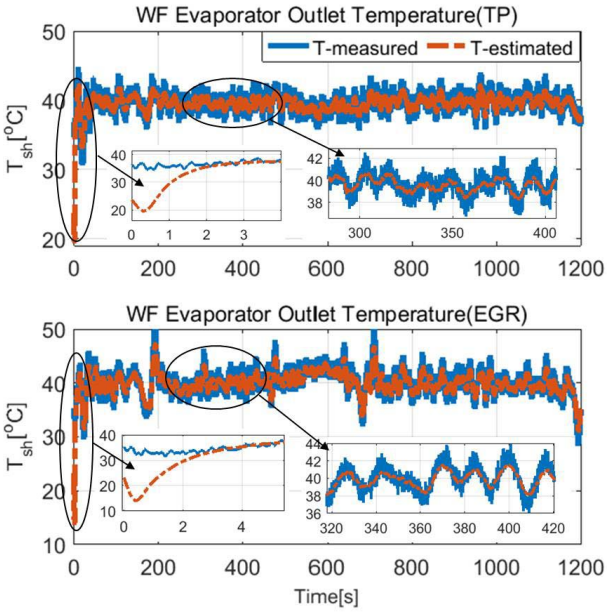

Fig. 8. Estimated and measured evaporator outlet WF temperature for both TP and EGR evaporators.

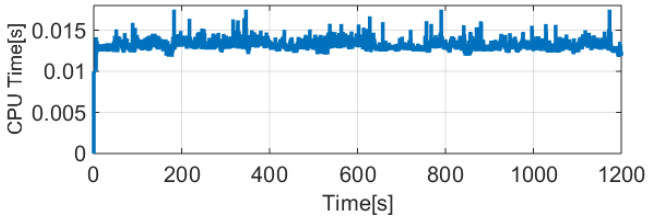

Fig. 9. NMPC computation time.

differences between the plant and control models as discussed in Section III. Namely, there is no one-to-one correlation of state variables between the plant model and control model except the evaporator temperatures constructed from the respective state variables.

The benefit of utilizing ACADO code generation for NMPC implementation is shown via the computational efficiency plotted in Fig. 9. For a feedback update sample time of 0.2 s, the NMPC takes a maximum of 0.018 s to calculate the control input, which is a realistic computation time for real-time implementation of the proposed control scheme. Note that the NMPC simulation is implemented in Simulink on a high-end 2015 Dell laptop (Intel(R) Core(TM) i7-4810MQ CPU@2.8GHZ, 8GB RAM, 1TB Hard Disk).

B. Performance Study of the Proposed Control Versus Conventional Multiple-Loop PID Control

The performance of the proposed control scheme is further examined in Fig. 10, where the normalized net power generated produced with the proposed control scheme relative to a conventional multiple-loop PID control is compared. In this simulation case, to maximize the power generation potential, the following simulation conditions are considered.

1) The turbine valve is allowed to be fully open whenever the WF vapor has a vapor quality greater than one. Simultaneously, the bypass valve is fully closed. However, the PID evaporation pressure controller is set to open the bypass valve in case of a safety concern defined by the maximum acceptable evaporating pressure.
2) The saturation temperature (T_{sat}) plus 15 °C of superheat is the reference considered for both control schemes. As discussed in the introduction, for a low latent energy WF, maximum ORC WHR power can be generated by operating close to saturation temperature. The 15 °C superheat buffer above saturation is considered to allow slight deviations in WF temperature from the reference trajectory due to transient engine exhaust conditions while still maintaining WF with a vapor quality greater than one for continuous power generation. As a reminder, operation of the turbine expander with nonsuperheated WF will result in component damage.

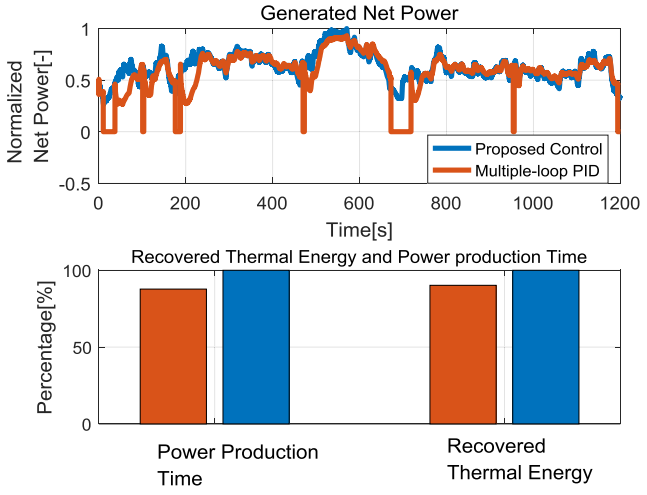

Fig. 10. Normalized net power production over the transient CSVL cycle (top), the corresponding time duration of operation in ORC power generation mode due to the presence of superheated vapor at the turbine inlet (bottom left), and the total recovered thermal energy (bottom right) by the proposed control and multiple-loop PID controllers, blue and orange, respectively.

As shown in Fig. 10, the vapor quality safety constraint is 100% satisfied by the proposed controller, which closely tracks the desired control reference and continuously generates power for the entire transient engine drive cycle. On other hand, the conventional, multiple-loop PID controller struggles to maintain the superheated vapor WF state in many instances, resulting in intermittent power generation due to closing and opening of the turbine valve.

In addition to smooth/continuous power generation over the given transient drive cycle, the performance of both controllers is quantified by calculating the total time in the superheated vapor state (t_{sv}) and the total recovered thermal energy (U_{thm}) over the entire CSVL drive cycle. The performance indicators are defined as follows:

$$t_{\text{sv}} = \sum_{t=0}^{t_f} t_s \text{ for } (v_q \geq 1) \tag{24a}$$

$$U_{\text{thm}} = \int_{t=0}^{t_{\text{sv}}} P_{\text{net}}(t)dt \tag{24b}$$

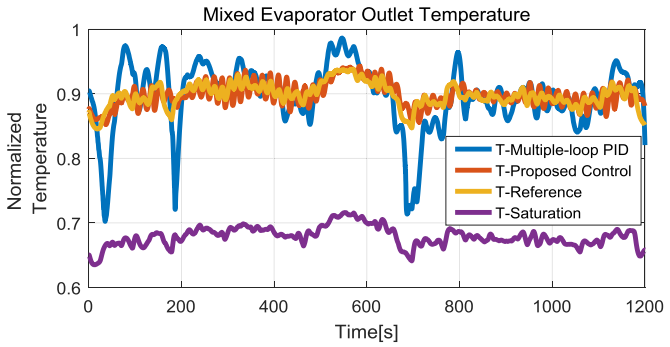

Fig. 11. Tracking profromance of mixed evaporator outlet WF temerature reference trajectory by proposed and multiple-loop PID controllers.

where $v_q = (h_{f,\text{out}} - h_{f,l})/(h_{f,g} - h_{f,l})$ is vapor quality calculated via WF enthalpy differences; the subscripts g and l refer to saturated vapor and saturated liquid states, respectively; t_f is the total cycle time; and t_s is the sample time for control updates. $P_{\text{net}} = P_{\text{Turb}} - P_{\text{Pump}}$ is the instantaneous net power calculated based on (8) and (9). In this net power calculation, the power consumption by the condenser coolant flow pump is neglected.

In Fig. 10, the relative percentage of time spent in ORC power production mode owing to the presence of superheated vapor at the turbine inlet is represented for both the proposed control and the coupled conventional PID controllers. The proposed controller maintains the ORC system in power production mode for the entire transient CSVL cycle, outperforming the conventional multiple-loop PID controller by 12%. In addition, Fig. 10 also displays the total recovered thermal energy during the transient CSVL cycle. Owing to the proposed controller's ability to produce power over more of the transient cycle, it enjoys a 9% gain in recovered thermal energy relative to the conventional multiloop PID.

To compare the tracking performance of both controllers (the proposed and the conventional multiple-loop PID), the power maximizing low superheat reference temperature trajectory ($T_{\text{sat}} + 15$ °C) is replaced by a relatively high temperature reference ($T_{\text{sat}} + 60$ °C), where both controllers are able to maintain superheated vapor production for the entire CSVL cycle. The relative tracking performance is shown in Fig. 11.

Superior WF temperature reference tracking performance (the mixed WF temperature from both evaporators at the inlet of the turbine expander) is achieved by the proposed control while the multiple-loop PID controller struggled to follow the desired trajectory. When an aggressive exhaust gas mass flow input change is introduced, the multiple-loop PID controller produces a large temperature over-shoot that drops toward saturation, while the proposed controller closely follows the desired temperature trajectory throughout. The large overshoot of the multiple-loop PID control is attributed to its poor disturbance rejection capability. Although superheated vapor production is maintained by both controllers for entire cycle CSVL cycle at this high superheat temperature reference ($T_{\text{sat}} + 60$ °C), the corresponding generated power is decreased by 13.8% (for the proposed control) and 14% (for the multiple-loop control) relative to the power generated at the low superheat reference temperature ($T_{\text{sat}} + 15$ °C) by the proposed controller. This confirms that maximum ORC power generation is obtained by operating near the WF saturation temperature to maximize the mass flowthrough the turbine. The proximity of the power maximizing temperature trajectory near the saturation safety boundary further highlights the need for extreme accuracy in temperature tracking.

Overall, the ability of the ORC controller to accurately track the desired temperature reference influences the level of superheat necessary to maintain ORC power generation during the entire cycle. Thus, the improved reference temperature tracking capability of the proposed controller relative to the conventional multiloop PID allows the proposed controller to operate at reference temperature trajectories closer to saturation while maintaining the WF in vapor state ahead of the turbine expander during transients, ultimately increasing the total ORC power generation.

VI. Conclusion

In this paper, an augmented control scheme of NMPC+UKF+PID is proposed for controlling a parallel evaporator ORC WHR system on a heavy duty engine. For computational tractability, the NMPC formulation is limited to controlling the mixed evaporator outlet WF temperature and the differential temperature between the parallel evaporator outlets. An external PID is designed for evaporator pressure control, assuming a separation between the thermal and pressure dynamics. The NMPC is updated by estimating the full system state via UKF. Both the NMPC and the UKF are designed based on a reduced order, control oriented, MB heat exchanger model. To meet real-time implementation constraints with the proposed controller, the NMPC is implemented using an efficient code generation tool ACADO, and an average computation time of less than 0.018 s is achieved for this ORC-WHR application.

The performance of the proposed control was demonstrated through simulations studies that consider a transient CSVL engine drive cycle while applying the control input over an experimentally validated, high fidelity, physics-based ORC plant model. A smooth control performance is observed both for the mixed evaporator outlet temperature and pressure control.

The proposed control was also compared with a conventional multiple-loop PID control for two cases of reference temperature trajectory tracking: low ($T_{\text{sat}} + 15$ °C) and high ($T_{\text{sat}} + 60$ °C) levels of superheat. Superior performance is achieved by the proposed controller in-terms of: temperature reference tracking, maintaining superheated vapor before the turbine expander over the entire CSVL cycle, and total thermal energy recovered. For the ($T_{\text{sat}} + 15$ °C) reference trajectory tracking case, simulation results with the proposed control show increases of 12% in total ORC power production time and 9% in total recovered thermal energy relative to the conventional multiple-loop PID control. Future work will consider driving cycles with even more aggressive transients. However, the net power benefits of a forward-looking control

strategy relative to conventional PID control are expected to increase directly with the drive cycle's transient severity.

The robustness of the proposed control is evaluated through consideration of a high fidelity plant model and a reduced order control model, which inherits modeling uncertainty due to its inherent simplifications. In the future, simulation studies will further explore the robustness of the proposed control considering parameter uncertainties for any potential dynamics not captured in the model. Future work also includes a performance evaluation of the augmented control scheme (NMPC+UKF+PID) on the experimental hardware, extending the preliminary experimental work published in [60] for single evaporator case.

The results and discussion in this paper focused on the relative power generation gains of the proposed control considering two cases of temperature reference trajectory while neglecting the effort to circulate fluid in the condensing circuit. In reality, the cooling effort will compromise the net power production from the ORC-WHR system. This will be quantified in the future work.

ACKNOWLEDGMENT

This research was conducted as part of a sponsored research contract between Clemson University and BorgWarner Inc.

REFERENCES

[1] H. Teng, "Waste heat recovery concept to reduce fuel consumption and heat rejection from a diesel engine," *SAE Int. J. Commercial Veh.*, vol. 3, no. 1, pp. 60–68, 2010.

[2] A. M. Noor, R. C. Puteh, and S. Rajoo, "Waste heat recovery technologies in turbocharged automotive engine—A review," *J. Mod. Sci. Technol.*, vol. 2, no. 1, pp. 108–119, 2014.

[3] K. Yazawa, Y. R. Koh, and A. Shakouri, "Optimization of thermoelectric topping combined steam turbine cycles for energy economy," *Appl. Energy*, vol. 109, pp. 1–9, Sep. 2013.

[4] F. Vélez, J. J. Segovia, M. C. Martín, G. Antolín, F. Chejne, and A. Quijano, "A technical, economical and market review of organic Rankine cycles for the conversion of low-grade heat for power generation," *Renew. Sustain. Energy Rev.*, vol. 16, no. 6, pp. 4175–4189, 2012.

[5] H. Teng, G. Regner, and C. Cowland, "Waste heat recovery of heavy-duty diesel engines by organic Rankine cycle part I: Hybrid energy system of diesel and Rankine engines," SAE Tech. Paper 2007-01-0537, 2007.

[6] C. Zhang, G. Q. Shu, H. Tian, H. Wei, G. Yu, and Y. Liang, "Theoretical analysis of a combined thermoelectric generator (TEG) and dual-loop organic Rankine cycle (DORC) system using for engines' exhaust waste heat recovery," SAE Tech. Paper 2014-01-0670, 2014.

[7] X. Liu, Y. D. Deng, S. Chen, W. S. Wang, Y. Xu, and C. Q. Su, "A case study on compatibility of automotive exhaust thermoelectric generation system, catalytic converter and muffler," *Case Stud. Thermal Eng.*, vol. 2, pp. 62–66, Mar. 2014.

[8] C. Liu and W. Z. Li, "An experimental study of a novel prototype for thermoelectric power generation from vehicle exhaust," *Distrib. Generat. Alternative Energy J.*, vol. 28, no. 4, pp. 32–48, 2013.

[9] I. Arsie, A. Cricchio, C. Pianese, M. De Cesare, and W. Nesci, "A comprehensive powertrain model to evaluate the benefits of electric turbo compound (ETC) in reducing CO_2 emissions from small diesel passenger cars," SAE Tech. Paper 2014-01-1650, 2014.

[10] Y. Ismail, D. Durrieu, P. Menegazzi, P. Chesse, and D. Chalet, "Study of parallel turbocompounding for small displacement engines," SAE Tech. Paper 2013-01-1637, 2013.

[11] K. K. Srinivasan, P. J. Mago, and S. R. Krishnan, "Analysis of exhaust waste heat recovery from a dual fuel low temperature combustion engine using an organic Rankine cycle," *Energy*, vol. 35, no. 6, pp. 2387–2399, 2010.

[12] D. Menniti, N. Sorrentino, A. Pinnarelli, A. Burgio, G. Brusco, and G. Belli, "The concentrated solar power system with Stirling technology in a micro-grid: The simulation model," in *Proc. Int. Symp. Power Electron., Elect. Drives, Autom. Motion (SPEEDAM)*, Jun. 2014, pp. 253–260.

[13] R. Patton and G. Bennett, "High efficiency internal combustion stirling engine development," SAE Tech. Paper 2011-01-0410, 2011.

[14] B. Song *et al.*, "An investigation on the performance of a Brayton cycle waste heat recovery system for turbocharged diesel engines," *J. Mech. Sci. Technol.*, vol. 27, no. 6, pp. 1721–1729, 2013.

[15] B. Song, W. Zhuge, X. Zheng, Y. Zhang, Y. Yin, and Y. Zhao, "Parameter study of a Brayton cycle waste heat recovery system for turbocharged diesel engines," in *Proc. ASME Fluids Eng. Division Summer Meet.*, 2013, p. V01CT18A006.

[16] T. Park, H. Teng, G. L. Hunter, B. van der Velde, and J. Klaver, "A Rankine cycle system for recovering waste heat from HD diesel engines—Experimental results," SAE Tech. Paper 2011-01-1337, 2011.

[17] H. Teng, G. Regner, and C. Cowland, "Achieving high engine efficiency for heavy-duty diesel engines by waste heat recovery using supercritical organic-fluid Rankine cycle," SAE Tech. Paper 2006-01-3522, 2006.

[18] H. Teng and G. Regner, "Improving fuel economy for HD diesel engines with WHR Rankine cycle driven by EGR cooler heat rejection," SAE Tech. Paper 2009-01-2913, 2009.

[19] B. Xu, X. Liu, J. Shutty, P. Anschel, S. Onori, Z. Filipi, and M. Hoffman, "Physics-based modeling and transient validation of an organic Rankine cycle waste heat recovery system for a heavy-duty diesel engine," SAE Tech. Paper 2016-01-0199, 2016.

[20] D. Seher, T. Lengenfelder, J. Gerhardt, N. Eisenmenger, M. Hackner, and I. Krinn, "Waste heat recovery for commercial vehicles with a Rankine process," in *Proc. 21st Aachen Colloq. Automobile Eng. Technol.*, 2012. [Online]. Available: http://hdl.handle.net/2268/147369

[21] O. Delgado and N. Lutsey, "The U.S SuperTruck program: Expediting the development of advanced heavy-duty vehicle efficiency technologies," Int. Council Clean Transp., White Paper, Jun. 2014.

[22] H. Teng, G. Regner, and C. Cowland, "Waste heat recovery of heavy-duty diesel engines by organic Rankine cycle part II: Working fluids for WHR-ORC," SAE Tech. Paper 2007-01-0543, 2007.

[23] H. Chen, D. Y. Goswami, and E. K. Stefanakos, "A review of thermodynamic cycles and working fluids for the conversion of low-grade heat," *Renew. Sustain. Energy Rev.*, vol. 14, no. 9, pp. 3059–3067, 2010.

[24] J. Bao and L. Zhao, "A review of working fluid and expander selections for organic Rankine cycle," *Renew. Sustain. Energy Rev.*, vol. 24, pp. 325–342, Aug. 2013.

[25] J. R. Juhasz and L. D. Simoni, "A review of potential working fluids for low temperature organic Rankine cycles in waste heat recovery," in *Proc. 3rd Int. Seminar ORC Power Syst. (ASME ORC)*, Brussels, Belgium, vol. 12. 2015, pp. 12–14.

[26] R. K. Shah and D. P. Sekulic, *Fundamentals of Heat Exchanger Design*. New York, NY, USA: Wiley, 2003.

[27] S. Saghlatoun, W. Zhuge, and Y. Zhang, "Review of expander selection for small-scale organic Rankine cycle," in *Proc. ASME 4th Joint U.S.-Eur. Fluids Eng. Division Summer Meet., ASME 12th Int. Conf. Nanochannels, Microchannels Minichannels*, 2014, p. V01BT10A041.

[28] J. Peralez, M. Nadri, P. Dufour, P. Tona, and A. Sciarretta, "Control design for an automotive turbine Rankine cycle system based on nonlinear state estimation," in *Proc. IEEE 53rd Annu. Conf. Decision Control (CDC)*, Dec. 2014, pp. 3316–3321.

[29] S. Quoilin, R. Aumann, A. Grill, A. Schuster, V. Lemort, and H. Spliethoff, "Dynamic modeling and optimal control strategy of waste heat recovery organic Rankine cycles," *Appl. Energy*, vol. 88, no. 6, pp. 2183–2190, 2011.

[30] J. Peralez *et al.*, "Improving the control performance of an organic Rankine cycle system for waste heat recovery from a heavy-duty diesel engine using a model-based approach," in *Proc. IEEE 52nd Annu. Conf. Decision Control (CDC)*, Dec. 2013, pp. 6830–6836.

[31] M. C. Esposito, N. Pompini, A. Gambarotta, V. Chandrasekaran, J. Zhou, and M. Canova, "Nonlinear model predictive control of an organic Rankine cycle for exhaust waste heat recovery in automotive engines," *IFAC-PapersOnLine*, vol. 48, no. 15, pp. 411–418, 2015.

[32] E. Feru, F. Willems, B. de Jager, and M. Steinbuch, "Model predictive control of a waste heat recovery system for automotive diesel engines," in *Proc. 18th Int. Conf. Syst. Theory, Control Comput. (ICSTCC)*, 2014, pp. 658–663.

[33] V. Grelet, P. Dufour, M. Nadri, V. Lemort, and T. Reiche, "Explicit multi-model predictive control of a waste heat Rankine based system for heavy duty trucks," in *Proc. 54th Annu. IEEE Conf. Decision Control (CDC)*, Osaka, Japan, Dec. 2015, pp. 179–184.

[34] G. Hou, R. Sun, G. Hu, and J. Zhang, "Supervisory predictive control of evaporator in organic Rankine cycle (ORC) system for waste heat recovery," in *Proc. Int. Conf. Adv. Mech. Syst. (ICAMechS)*, Aug. 2011, pp. 306–311.

[35] A. Hernandez, A. Desideri, C. Ionescu, S. Quoilin, V. Lemort, and R. De Keyser, "Increasing the efficiency of organic Rankine cycle technology by means of multivariable predictive control," *IFAC Proc. Volumes*, vol. 47, no. 3, pp. 2195–2200, 2014.

[36] T. Yamamoto, T. Furuhata, N. Arai, and K. Mori, "Design and testing of the organic Rankine cycle," *Energy*, vol. 26, no. 3, pp. 239–251, 2001.

[37] B. Xu, A. Yebi, S. Onori, Z. Filipi, X. Liu, J. Shutty, P. Anschel, and M. Hoffman, "Transient power optimization of an organic Rankine cycle waste heat recovery system for heavy-duty diesel engine applications," *SAE Int. J. Alternative Powertrains*, vol. 6, no. 1, pp. 25–33, 2017.

[38] B. Xu, A. Yebi, S. Onori, Z. Filipi, X. Liu, J. Shutty, P. Anschel, and M. Hoffman, "Power maximization of a heavy duty diesel organic Rankine cycle waste heat recovery system utilizing mechanically coupled and fully electrified turbine expanders," in *Proc. ASME Int. Combustion Eng. Division Fall Tech. Conf. (ICEF)*, Greenville, SC, USA, Oct. 2016, p. V001T05A005, paper 2016-9378.

[39] A. Hernandez, A. Desideri, C. Ionescu, R. De Keyser, V. Lemort, and S. Quoilin, "Real-time optimization of organic Rankine cycle systems by extremum-seeking control," *Energies*, vol. 9, no. 5, p. 334, 2016.

[40] J. Peralez, P. Tona, M. Nadri, P. Dufour, and A. Sciarretta, "Optimal control for an organic Rankine cycle on board a diesel-electric railcar," *J. Process Control*, vol. 33, pp. 1–13, Sep. 2015.

[41] A. Hernandez, A. Desideri, C. Ionescu, S. Quoilin, V. Lemort, and R. De Keyser, "Experimental study of predictive control strategies for optimal operation of organic Rankine cycle systems," in *Proc. Eur. Control Conf. (ECC)*, Jul. 2015, pp. 2254–2259.

[42] A. Yebi, B. Xu, X. Liu, J. Shutty, P. Anschel, S. Onori, Z. Filipi, and M. Hoffman, "Nonlinear model predictive control strategies for a parallel evaporator diesel engine waste heat recovery system," in *Proc. ASME Dyn. Syst. Control Conf.*, Minneapolis, MN, USA, 2016, p. V002T19A003.

[43] B. Houska, H. J. Ferreau, and M. Diehl, "ACADO toolkit—An open-source framework for automatic control and dynamic optimization," *Optim. Control Appl. Methods*, vol. 32, no. 3, pp. 298–312, 2011.

[44] A. H. Jazwinski, *Stochastic Processes and Filtering Theory*. New York, NY, USA: Dover, 2007.

[45] S. J. Julier, J. K. Uhlmann, and H. F. Durrant-Whyte, "A new approach for filtering nonlinear systems," in *Proc. Amer. Control Conf.*, Jun. 1995, pp. 1628–1632.

[46] S. J. Julier and J. K. Uhlmann, "A general method for approximating nonlinear transformations of probability distributions," Robot. Res. Group, Dept. Eng. Sci., Univ. Oxford, Oxford, U.K., Tech. Rep., 1996.

[47] S. Julier, J. Uhlmann, and H. F. Durrant-Whyte, "A new method for the nonlinear transformation of means and covariances in filters and estimators," *IEEE Trans. Autom. Control*, vol. 45, no. 3, pp. 477–482, Mar. 2000.

[48] K. Xiong, C. W. Chan, and H. Y. Zhang, "Detection of satellite attitude sensor faults using the UKF," *IEEE Trans. Aerosp. Electron. Syst.*, vol. 43, no. 2, pp. 480–491, Apr. 2007.

[49] R. Kandepu, B. Foss, and L. Imsland, "Applying the unscented Kalman filter for nonlinear state estimation," *J. Process Control*, vol. 18, nos. 7–8, pp. 753–768, 2008.

[50] B. Ristic *et al.*, "Performance bounds and comparison of nonlinear filters for tracking a ballistic object on re-entry," *IEE Proc.-Radar, Sonar Navigat.*, vol. 150, no. 2, pp. 65–70, Apr. 2003.

[51] N. Haverbeke *et al.*, "Nonlinear model predictive control with moving horizon state and disturbance estimation—Application to the normalization of blood glucose in the critically ill," *IFAC Proc. Volumes*, vol. 41, no. 2, pp. 9069–9074, 2008.

[52] E. Feru, F. Willems, B. de Jager, and M. Steinbuch, "Modeling and control of a parallel waste heat recovery system for Euro-VI heavy-duty diesel engines," *Energies*, vol. 7, no. 10, pp. 6571–6592, 2014.

[53] J. M. Michael and N. S. Howard, *Fundamentals of Engineering Thermodynamics*, 5th ed. New York, NY, USA: Wiley, 2006.

[54] J. M. Jensen, "Dynamic modeling of Thermo–Fluid systems with focus on evaporators for refrigeration," Ph.D. dissertation, Dept. Mech. Eng., Tech. Univ. Denmark, Lyngby, Denmark, 2003.

[55] E. F. Camacho and C. A. Bordons, *Model Predictive Control in the Process Industry*. New York, NY, USA: Springer, 2012.

[56] J. V. Frasch *et al.*, "An auto-generated nonlinear MPC algorithm for real-time obstacle avoidance of ground vehicles," in *Proc. Eur. Control Conf.*, Zurich, Switzerland, Jul. 2013, pp. 4136–4141.

[57] K. Xiong, H. Y. Zhang, and C. Chan, "Performance evaluation of UKF-based nonlinear filtering," *Automatica*, vol. 42, no. 2, pp. 261–270, 2006.

[58] R. Quirynen, M. Vukov, and M. Diehl, "Auto generation of implicit integrators for embedded NMPC with microsecond sampling times," *IFAC Proc. Volumes*, vol. 45, no. 17, pp. 175–180, 2012.

[59] B. Xu, D. Rathod, S. Kulkarni, A. Yebi, Z. Filipi, S. Onori, and M. Hoffman, "Transient dynamic modeling and validation of an organic Rankine cycle waste heat recovery system for heavy duty diesel engine applications," *Appl. Energy*, vol. 205, pp. 260–279, Nov. 2017.

[60] X. Liu, A. Yebi, P. Anschel, J. Shutty, B. Xu, M. Hoffman, and S. Onori, "Model predictive control of an organic Rankine cycle system," *Energy Procedia*, vol. 129, pp. 184–191, Sep. 2017.

Adamu Yebi received the B.S. degree in mechanical engineering from Bahir Dar University, Bahir Dar, Ethiopia, in 2005, the M.S. degree in sustainable energy engineering and mechanical design from the Royal Institute of Technology, Stockholm, Sweden, in 2011, and from Addis Ababa University, Addis Ababa, Ethiopia, in 2010, and the Ph.D. degree in automotive engineering from Clemson University, Clemson, SC, USA, in 2015.

He is currently a Post-Doctoral Research Associate with the Powertrain Research Group, International Center for Automotive Research, Clemson University. His current research interests include dynamic modeling, advanced controls, estimation, optimization, automation and testing for automotive-related applications, and advanced light weight manufacturing.

Dr. Yebi is a member of the ASME.

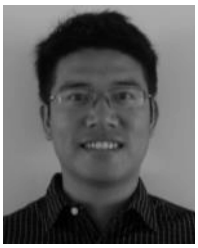

Bin Xu received the bachelor's degree in automotive engineering from Hunan University, Changsha, China, in 2013, and the Ph.D. degree in automotive engineering from Clemson University, Clemson, SC, USA, in 2017, with a thesis on the plant modeling, model reduction, and power optimization for an organic Rankine cycle waste heat recovery system in heavy duty diesel engine applications.

Since 2017, he has been a Post-Doctoral Researcher with Clemson University. His current research interests include organic Rankine cycle waste heat recovery system physics-based modeling, experimental verification, and model reduction for model-based control and power optimization.

Xiaobing Liu received the B.S. degree in thermal engineering from Tsinghua University, Beijing, China, in 1994, and the M.S. degree in electrical engineering and the Ph.D. degree in mechanical engineering from Michigan State University, East Lansing, MI, USA, in 1999 and 2001, respectively.

He is currently a Technical Specialist of controls and simulation with the Advanced Engineering Department, BorgWarner Inc., Auburn Hills, MI, USA. His current research interest includes control and simulation of hybrid electric vehicle, turbocharger and EGR system, engine stop/start, waste heat recovery, and transmission system.

John Shutty received the master's degree in systems engineering from Case Western Reserve University, Cleveland, OH, USA.

He was a Director of Controls at Cummins, Columbus, IN, USA. He is currently a Chief Engineer of Advanced Controls and Simulation with BorgWarner Inc., Auburn Hills, MI, USA.

Paul Anschel received the bachelor's degree from Swarthmore College, Swarthmore, PA, USA, and the master's degree in mechanical engineering from Colorado State University, Fort Collins, CO, USA.

He is currently a Senior Technical Specialist with the Corporate Advanced Engineering team, BorgWarner Inc., Auburn Hills, MI, USA, where he served as the Project Leader for BorgWarners Global Development teams for ORC and Thermoelectric Waste Heat Recovery since 2014. He served as the Director of Global Commercial Vehicle Product Development for BorgWarner Turbo. He was with Magneti Marelli, Inc., Sanford, NC, USA, and Sturman Industries, Woodland Park, CO, USA. He was involved in commercial vehicle and automotive product development for turbochargers, gasoline and diesel fuel injectors, fuel system, and air system products.

Zoran Filipi received the Ph.D. degree in mechanical engineering from the University of Belgrade, Belgrade, Serbia, in 1992.

He was with the University of Michigan, Ann Arbor, MI, USA, until 2011, where he rose to the rank of Research Professor. He is currently a Professor, a Timken Endowed Chair of Vehicle System Design, and a Chair with the Automotive Engineering Department, Clemson University (CU), Clemson, SC, USA. He also serves as an Executive Director with the Campbell Graduate Engineering Center, Greenville, SC, USA, the academic anchor of the CU International Center for Automotive Research. He has authored over 205 refereed papers and holds three patents. His current research interests include advanced IC engine concepts, alternative and hybrid powertrain systems, and energy for transportation.

Dr. Filipi is an SAE fellow and an ASME fellow. He was a recipient of the SAE Forest R. McFarland Award and the IMechE Donald Julius Groen Award, among others. He is the Editor-in-Chief of the SAE Journal of Alternative Powertrains.

Simona Onori received the Laurea (*summa cum laude*) degree in computer science and engineering from the University of Rome "Tor Vergata", Rome, Italy, in 2003, the M.S. degree in electronics and communication engineering from the University of New Mexico, Albuquerque, NM, USA, in 2004, and the Ph.D. degree in control engineering from the University of Rome "Tor Vergata" in 2007,

She has been an Assistant Professor with the Clemson University International Center for Automotive Research, Clemson, SC, USA, since 2013, where she also holds a joint apportionment with the Electrical and Computer Engineering. She was a Visiting Professor at the University of Trento, Trento, Italy, in 2014, at the Beijing Institute of Technology, Beijing, China, in 2015, and at the University of Orleans, Orleans, France, in 2016.

Dr. Onori was a recipient of the 2017 NSF CAREER Award, the 2017 Clemson University College of Engineering and Science Dean's Faculty Fellows Award, the 2017 Clemson University Esin Gulari Leadership and Service Award, the 2016 Energy Leadership Award in the category Emerging Leader (for the Carolinas), the 2015 Innovision Award at South Carolina, and the 2012 Lumley Interdisciplinary Research, 2011 Outstanding Technology Team Award, TechColumbus. She is a PSG Distinguished Visiting Professor awarded by the Managing Trustee of PSG College of Technology, Coimbatore, India, in 2017.

Mark Hoffman received the B.S. (*summa cum laude*) degree in mechanical engineering from Union College, Schenectady, NY, USA, in 2003, and the M.S. and Ph.D. degrees from the Department of Mechanical Engineering, University of Michigan, Ann Arbor, MI, USA, in 2008 and 2012, respectively.

He has been a Research Assistant Professor with the Department of Automotive Engineering, Clemson University, Clemson, SC, USA, since 2013, where he also serves as the Director of Clemson's Automotive Engineering Certificate program. His current research interests include low-temperature combustion, heat transfer, thermal barrier coatings, combustion chamber deposits, waste heat recovery, vehicle energy management, catalytic emissions systems, particulate emissions mitigation, and gasoline particulate filters.